Proceedings of the 1999 IEEE/ASME
International Conference on Advanced Intelligent Mechatronics
September 19-23, 1999 • Atlanta, USA

Force Controlled Pushing of Nanoparticles: Modeling and Experiments

Metin Sitti and Hideki Hashimoto
Institute of Industrial Science, University of Tokyo
Roppongi, 7-22-1, Minato-ku, Tokyo, 106-8558, Japan

***Abstract*— In this paper, a nano-robotics manipulation system using Atomic Force Microscope (AFM) probe as the pushing manipulator and force and topology sensor has been proposed. The task is the 2-D positioning of nanometer size particles on a substrate in ambient conditions. Thus, the modeling of interaction forces and dynamics during pushing operation is analyzed for understanding the nano scale physical phenomenon which is different from macro robotics physics. Simulations and experiments are held for determining the conditions and strategy for reliable manipulation, and determining the affecting parameters. The results show that latex particles can be positioned on silicon substrates successfully.**

1 Introduction

Nanotechnology which aims at the ideal miniaturization of devices and machines down to atomic and molecular sizes has been a recent hot topic as a promising high-technology for the forthcoming century. By precise control of atoms, molecules or nano scale objects, new sensors and man-made materials, tera-byte capacity memories, micro scale robots/machines, DNA-computers, quantum devices, micro scale distributed intelligence system devices with integrated sensors, actuators and communication tools, etc. would be possible within the near future. However, for new nanotechnology products, still there are many challenges to be solved, and nano manipulation is one of the important challnges at the nano world. This kind of research is still immature since the physical and chemical phenomenon at this scale has not been completely understood, intelligent automatic precision manipulation strategies are not developed, and the specific tools for the specific applications have not been defined/designed clearly. Thus, the purpose of this paper is to propose an Atomic Force Microscope (AFM)-based force controlled pushing system with physical analysis of the manipulation tool (AFM tip) and nano scale object physical interaction for 2-D positioning and assembly of nanoparticles.

AFM is a 3-D atomic resolution microscope which uses the interatomic force measurement principle for helding the topology images. Its mechanicsm is mechanical, and can be applied to imaging of all types of particles/samples which are fully or semi-fixed on a substrate with homogenous surface stiffness and interatomic force properties. Changing its function from only imaging to both imaging and manipulation, new challenging problems are introduced. At first, the particles on substrates should be *semi-fixed* in order to be able to move them. The solution to this problem could be using non-contact mode AFM imaging for not moving the particles during imaging as proposed by [15]. However, the selection of the absorption chemicals is a difficult issue depending on the type of the substrate and particle (for Au particles, Silane is used for silicon subtrates [9], and Ploy-L-Lysine for mica substrates [11]). Next, the mechanism of interatomic forces and dynamics should be understood for precise positioning of the particles [13]. However, the micro/nano mechanics for this kind of application has not been developed completely. Moreover, real-time monitoring of the manipulation process is almost impossible. Since the same tool is used as either the imaging or manipulation tool at an instant, imaging is not possible during pushing operation. As one approach to this problem, researchers scan the area, where the target particle is, before and after the manipulation [2], [7], [12], [4]. Thus, by using some fixed reference features, the new relative position of the particle is obtained from the images. However, this imaging is still off-line and the problems during pushing cannot be understood by this way. On the other hand, the other way is utilizing the force feedback information during pushing for reliable manipulation [16], [17]. Another approach may be using high-resolution external Scanning Electron Microscope imaging [8] while this can be done only in vacuum environments, tip and particle can be obscured, and only some specific particles can be imaged by this way.

In this paper, possible solutions are proposed for the above challenging problems of AFM-based pushing. Force and dynamics modeling of the pushing operation, using real-time force feedback instead of real-time visual feedback or another external microscope during pushing, and using non-contact (tapping) imaging mode for imaging, and contact-mode for pushing are to be realized. A home-made AFM system with piezoresistive detection is constructed, and simulation and experimental results are compared for latex particle pushing applications.

0-7803-5038-3/99/$10.00 © 1999 IEEE

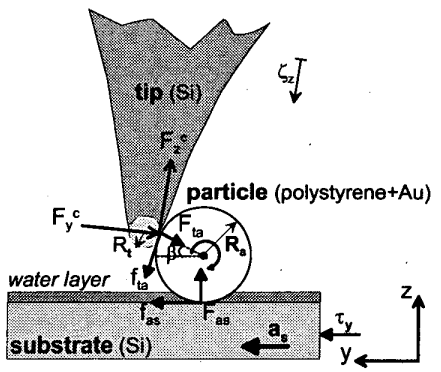

Figure 1: Positioning of the nano particles by the AFM tip contact pushing.

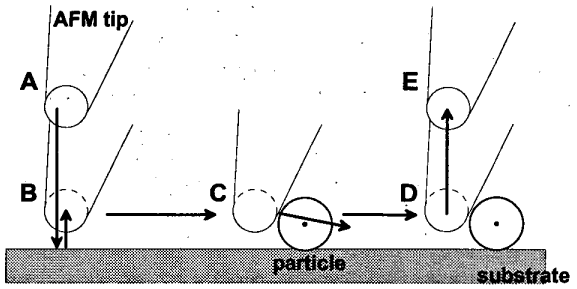

Figure 2: AFM-based particle pushing strategy.

2 Physical Modeling of 2-D Nano Particle Manipulation

In this paper, gold-coated latex particles absorbed on silicon substrates are to be pushed using a silicon fabricated AFM cantilever tip in ambient conditions as shown in Figure 1.

2.1 Manipulation Strategy

AFM-based pushing is realized by the motion steps as shown in Figure 2.

- $A \rightarrow B$ (*auto-parking*): the tip is automatically moved at z-direction until detecting the contact by the substrate by measuring the cantilever deflection (absolute tip-substate distance is not known initially), and retracted back to a predetermined parking position,
- $B \rightarrow C$ (*auto-particle contact detection*): the tip is moved along the substrate until detecting the particle by cantilever deflection detection, and then stopped,
- $C \rightarrow D$: pushing the particle for a desired distance by moving the tip or the substrate with a constant speed,
- $D \rightarrow E$: after completing the pushing operation, retracting back to the initial height.

2.2 Interaction Forces in Air

The interatomic force $F_z(t)$ between the AFM tip and elactic sample which is perpendicular to the cantilever is attractive or repulsive. Gravitational forces are relatively very small, and therefore negligible. These forces should be understood in order to control them for precise manipulation and interpret the cantilever deflection curves. A typical deflection curve of the cantilever depending on the tip-sample distance is shown in Figure 3 for a silicon AFM tip and silicon flat sample. The main components of the interatomic forces are van der Waals, capillary, electrostatic and indentation/repulsive forces. These forces are to be analyzed for modeling the tip-sample interaction. As the notation, the (-) force means the attractive and (+) do repulsive forces.

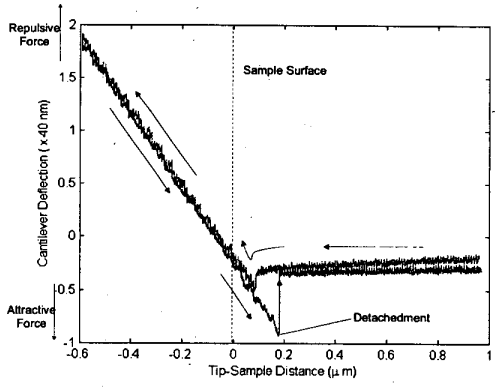

Figure 3: The typical cantilever deflection, i.e. interatomic force, and tip-sample distance relation.

2.2.1 Van der Waals Forces

It exists for every material in every environmental condition (like the gravitational force in the macro world), and depends on the object geometry, material type and relative distance. Assuming the interaction of the spherical cantilever tip with a spherical absorbate/particle, the exact additive solution becomes as [1]:

$$F_{vdw}^{ta}(h) = -\frac{H(h+r_+)}{3}\left\{\frac{2R_aR_t}{h^2(h+2r_+)^2} + \frac{2R_aR_t}{((h+r_+)^2-r_-^2)^2} + \frac{1}{h(h+2r^+)} - \frac{1}{(h+r^+)^2-r_-^2}\right\}, \quad (1)$$

where $r_+ = R_t + R_a$, $r_- = R_t - R_a$, R_t and R_a are the tip and particle radius respectively, $h = h(t)$ is the tip-particle distance, and H is the Hamacker constant. In most cases, $h >> R_a$ kind of assumption is made for micro particles, but for the nanoparticles, exact solution would be more proper. Since there is always a liquid (water) layer on the sample in air conditions, $H = \{(H_{tip} - H_{liquid})(H_{particle} - H_{liquid})\}^{1/2}$ [6]. For the particle-substrate interaction, van der Waals force becomes as:

$$F_{vdw}^{as}(h) = -\frac{H}{6}\left\{\frac{R_a}{h^2} + \frac{R_a}{(h+2R_a)^2} - \frac{1}{h} + ln\frac{1}{(h+2R_a)}\right\} \quad (2)$$

2.2.2 Capillary Forces

For the capillary force between the tip and particle, including solid-solid adhesion force $F_{s-s}^{ta} = 2\pi\tilde{R}\gamma_{SL}$,

$$F_{cap}^{ta}(h) = -\frac{2\pi\tilde{R}\gamma_L}{1+\frac{h-a_0}{2r_1}}u(h-L) - F_{s-s}^{ta} \ , \quad (3)$$

where $\tilde{R} = R_t R_a/(R_t + R_a)$ using the Derjaguin approximation, r_1 is the meniscus curvature radius (r_1 can be approximated as $r_1 \approx -0.54/log(P/P_s)(nm)$ using Kelvin equation [6] assuming a water layer at $20C^o$ where P/P_s is the relative humidity ratio), $L = L_l$ during approaching and $L = \delta$ during retraction where $L_l \approx 2r_1$ is the thickness of the water layer, and δ is the breaking length of the meniscus which is determined by the JKR contact mechanics modeling as $\delta = 0.132(6\pi\tilde{R}^{1/2}\gamma_L/K)^{2/3}$ where $1/K = [(1-\nu_t^2)/E_t + (1-\nu_a^2)/E_a]$, and E_t and E_a are the Young modulus, and ν_t and ν_s are the Poison's coefficients of the tip and particle respectively. γ_L is the liquid surface energy (for water $\gamma_L = 72mJ/m^2$), and γ_{SL} is the surface energy between solid-liquid interface. Often $\gamma_L > \gamma_{SL}$, and the F_{s-s} force can be ignored.

For the particle and substrate, i.e. F_{cap}^{as}, above equations are changed such that $\tilde{R} \to R_a$, $F_{s-s}^{ta} \to F_{s-s}^{as}$, and $\gamma_L \to 2\gamma_L$ where $F_{s-s}^{ta} = F_{s-s}^{as}$ in our case.

2.2.3 Electrostatic Forces

Grounding a (semi)conducting substrate such as Si, Au or HOPG, the electrostatic forces are reduced. However, in the case of polystyrene latex particles, there are charges trapped around the perimeter of the particles, and during pushing or contact, triboelectrification introduces local charges. Since the particles are not picked up, the electrostatic force between the particle and substrate is not important. But, after pushing, the charge on the particle is transfered to the tip which can cause an electrostatic force between the particle and tip (then particles can stick to the tip during retraction which is observed in some cases experimentally). As solution to this problem, the latex particles are coated with Au, and by grounding all the substrate and particles, electrostatic forces can be negligible. However, still a model for the electrostatic forces is desirable for general cases.

It is assumed that the all objects are free of charge at the beginning. But, after contacting with the objects, contact electrification and triboelectrification occurs, and forces due to these charges should be computed.

For the work functions of ϕ_1 and ϕ_2 of two surfaces, resulting voltage difference is $U = (\phi_1 - \phi_2)/e$ where $e = 1.6\times10^{-19}\ C$ is the e^- charge. Then the electrostatic force becomes as:

$$F_{el}(h) = -\frac{\epsilon_0 U^2 S}{2h^2} \ , \quad (4)$$

where ϵ_0 is the permittivity, and S is the shared area. For the tip-particle interaction, $S = 4\pi\tilde{R}r_1$, and $U = 0.25\ V$ for gold-coated particle surface and silicon tip. For the gold-coated particle and silicon substrate, $S = 4\pi R_a r_1$, and $U = 0.5\ V$. Then for $R_t = 30\ nm$, $R_a = 250\ nm$, $r_1 = 1.7\ nm$, and $h < 10\ nm$, F_{el}^{ta} is in the order of 10s of pN which can be almost neglected.

2.2.4 Indentation/Repulsive Forces

Since the contact area between the particle and tip is very small, only the deformation between the particle and substrate along the z-axis is considered [19]. Assuming still in the range of continuum mechanics, JKR contact model [14] is selected for approximate contact area prediction. Adding the short-ranged adhesion forces, for spherical tip and flat surface, JKR model results in the following equations:

$$\begin{aligned} P_z &= Ka^3/R_a - \sqrt{3\pi\omega K a^3} \\ \delta &= a^2/R_a - 2/3\sqrt{3\pi\omega a/K} \\ a^3 &= R_a/K(P_z + 3\pi R_a\omega + \sqrt{6\pi R_a\omega P_z + (3\pi R_a\omega)^2}) \end{aligned} \quad (5)$$

where P_z is the applied load along the z-axis, ω is the adhesion energy, and a is the contact radius.

2.2.5 Frictional Forces

During pushing, the friction between the particle and substrate plays an important role. The definition of the friction at the micro/nano scale can be given as:

$$f_{as} = \mu_{as}(A_{as} + F_l^{as}) \ , \quad (6)$$

where $A_{as} = 4\pi R_a\gamma_L$ is the adhesion force, and F_l^{as} is the external load. Also, there is a friction between the tip and particle such that

$$f_{ta} = \mu_{ta}(A_{ta} + F_l^{ta}) \ , \quad (7)$$

with $A_{ta} = 2\pi\tilde{R}\gamma_L$.

2.3 Sample Preparation

Preparation of dispersed nanoparticles is a challenging issue, and JEOL Co. particles which are dispersed with a scattering gun on a silicon substrate is utilized for the experiments.

As the design issue, the above forces should be checked for the selected particle and substrate geometry and material type, and environmental conditions such that:

- during tip-particle approach and separation, the adhesion forces should not result in sticking of the particles to the tip,
- static frictional forces should be smaller than the applied load in order to be able to move a particle.

More detailed analysis results in following conditions for helding above features:

$$R_a > 0.5\tilde{R}sin\beta \ , \tag{8}$$

$$\mu^s_{as} \geq \frac{\tilde{R}cos\beta}{2R_a} = \frac{cos\beta}{2(1+R_a/R_t)} \ . \tag{9}$$

where μ^s_{as} is the static friction coefficient for particle-substrate interaction. First equality is always correct which shows the advantage of the sharp parabolic (spherical) tip apex structure. For the second one μ^s_{as} is calculated depending on R_a where $R_t = 30\ nm$ is fixed in our system. For $R_a = 10\ nm$, $\mu^s_{as} \geq 0.014$, and for $R_a = 1000\ nm$, $\mu^s_{as} \geq 0.35$. Here, μ_s cannot be selected arbitrarily since then the particle may not be pushed. For reducing this problem, μ^s_{as} should be selected as $\mu^s_{as} \approx cos\beta/2(1+R_a/R_t)$, and a stiff cantilever should be used for enough pushing load.

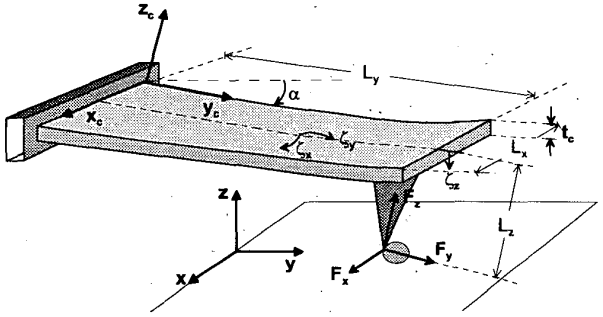

Figure 4: Cantilever bending along x-y-z axes during pushing nano objects.

2.4 Cantilever Dynamics and Position Control

Denoting the deflections along the x, y and z axes as ζ_x, ζ_y and ζ_z respectively as shown in Figure 4, the deflection vector is defined as $\zeta = [\zeta_x\ \zeta_y\ \zeta_z]^T$. Taking the force vector as $\mathbf{F} = [F_x\ F_y\ F_z]^T$, and assuming the cantilever with the normal stiffness of k_c is tilted by an angle of α along the x-axis, the deflection is determined by the forces as follows [3]:

$$\zeta = \mathbf{CF}$$

$$\mathbf{C} = \frac{1}{k_c}\begin{bmatrix} c_1 & 0 & 0 \\ 0 & c_2 & c_3 \\ 0 & c_3 & 1 \end{bmatrix} \tag{10}$$

where $c_1 = 2L_z^2/L_y^2 + t_c^2/L_x^2$, $c_2 = 3L_z^2/L_y^2$, $c_3 = 3L_z/(2L_y)$, L_x, $L_y and\ L_z$ are the cantilever lengths along the x-y-z axes, and t_c is the cantilever thickness. Thus, the important point is, the cantilever cannot be modeled as three decoupled springs for an accurate modeling where y and z axes are coupled. Using our piezoresistive deflection measurement system, only ζ_z can be measured (also ζ_x can be measured if the optical detection method is utilized which is our future work). Then, the measured deflection corresponds to:

$$\zeta_z = (c_3F_y + F_z)/k_c \ . \tag{11}$$

Thus, the lateral force of F_y has also affect on ζ_z. Assuming the change of the normal force is negligible during the pushing operation, the change in F_y, i.e. ΔF_y, can be computed as:

$$\Delta F_y = k_c\Delta\zeta_z/c_3 \ . \tag{12}$$

This means that the F_y frictional force component corresponding to the applied pushing load can be observed from ζ_z directly.

Piezoelectric XYZ actuators are utilized for atomic resolution positioning. These actuators have hystheresis and drift problems depending on the motion duration and range, and temperature changes. For imaging, since xy motion consists of scanning with specified constant range, actuators can be calibrated off-line using laser interferometry, and these calibration data are then can be used for accurate scanning (in the case of commercial AFMs). However, in manipulation tasks, the tip moves on arbitrary user-defined or automatic points in a given range; thus, open-loop control is almost not reliable. Therefore, the best is to integrate high resolution sensors such as capacitive, strain gauge, LVDT, or optical sensors to motion axes for closed-loop control. In our system, a Physick Instrumente XYZ closed-loop stage (P-762.3L) with 10 nm resolution, 0.1 % hystheresis error and 100μm range in all axes is utilized. The dynamics of the stage along the y-axis can be given as [5]:

$$\frac{1}{\omega_y^2}\ddot{y}_s + \frac{1}{\omega_y Q_y}\dot{y}_s + y_s = \tau_y - f_{as} \ , \tag{13}$$

where $\omega_y = 2\pi f_y$, $f_y = \sqrt{k_y/m_s}/(2\pi) = 250\ Hz$ is the y-stage resonant frequency with m_s and k_y are the stage and sample total mass and k_y is the y-axis stage stiffness, $Q_y = 20$ is the amplification factor, y_s denotes the sample y-axis position, and τ_y is the stage driving force.

2.5 Pushing Mechanism

For simplifying the notations and graphs, the particle is assumed to be pushed along y-axis where same notation and models can be extended to the x-y motion case directly. The interacting forces during pushing are shown in Figure 5. The parameters shown in the model

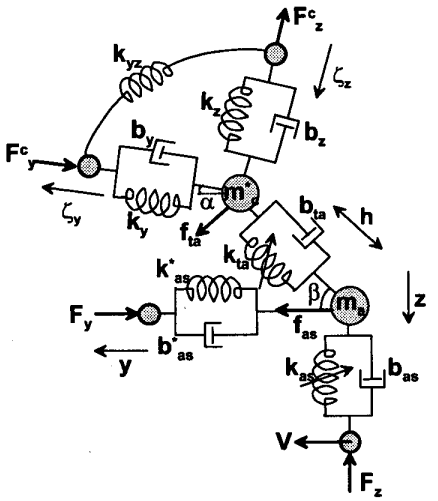

Figure 5: Point-mass model of the contact pushing mechanism along the y-axis.

are given as follows: $k_z = k_c$, $k_y = k_c/c_2$, $k_{xy} = k_c/c_3$, $b_z = b_y = 2\pi f_r m^*_c/Q_c$ where f_r is the cantilever resonant frequency and Q_c is the quality factor in air, $m^*_c = k_z/(4\pi^2 f_r)$ is the cantilever effective mass, m_a is the particle mass, $V = dy_s/dt$ is the *constant* y-stage speed, h is the tip-particle indentation depth, $k^*_{as} = 8R_aG^*$ with $G^* = ((2-\nu_a)/G_a + (2-\nu_s)/G_s)^{-1}$ where G_a and G_s are the shear modulus for the particle and substrate respectively, $k_{ta} = -\partial F_{ta}/\partial h$, b_{ta} is the tip-particle damping term which is negligible, $k_{as} = -\partial F_{as}/\partial z$, b_{as} is the particle-substrate damping, $k^*_{as} = 0.85k_{as}$ [10], and $b^*_{as} \approx 0$.

During the pushing operation, there are two main phases: static friction and kinetic friction regions. At the beginning, due to the satic friction, the particle and tip follow the stage motion along y-axis until to the point where the applied cantilever load exceeds the static friction between the particle and substrate. In this region following equations are held at the equilibrium points assuming a slow motion:

$$\begin{aligned}
&f_{as} = F^c_y cos\alpha + F^c_z sin\alpha \ , \\
&f_{as} = \mu^s_{as}(y)(F_{as} + A_{as} \ , \\
&F_{as} = F^c_y sin\alpha - F^c_z cos\alpha \ , \\
&F^c_y = k_y y cos\alpha \ , \\
&F^c_z = k_z y sin\alpha \ , \\
&F_y = k^*_{as} y \ . \qquad (14)
\end{aligned}$$

Here, $\zeta_y \approx ycos\alpha$, $\zeta_z \approx ysin\alpha$, $y = y_s$, $z = \delta$ from the JKR model using Eq. (5) with $P_z = F_{as}$. At the shearing point $y = y^*$, $f_{as} = \mu^s_{as}(F_{as}(y^*) + A_{as}) = F_y(y^*)cos\alpha + F_z(y^*)sin\alpha$. Then y^* can be computed as

$$y^* = \frac{\mu^s_{as} 4\pi R_a \gamma_L}{k_y cos^2\alpha + k_z sin^2\alpha - \mu_s sin\alpha cos\alpha (k_y - k_z)} \ . \qquad (15)$$

From this relation, the condition for enabling the particle pushing can be given as $y^* \geq 0$ which means that $\mu^s_{as} \leq (k_y cot\alpha + k_z tan\alpha)/(k_y - k_z)$. For example, for $\alpha = 15^o$, $k_z = 8\ N/m$ and $k_y = 1427\ N/m$, $\mu^s_{as} \leq 3.45$. Connecting this equality with Eq. (9):

$$\frac{cos\beta}{2(1+R_a/R_t)} \leq \mu^s_{as} \leq \frac{k_y cot\alpha + k_z tan\alpha}{k_y - k_z} \ . \qquad (16)$$

After the particle is separated from the substrate surface, following cases may occur: pure sliding, stick-slip motion and rolling. At this phase, $f_{as} = \mu^k_{as} F_{as}$ where μ^k_{as} is the kinetic friction coefficient, and the main dynamics of the particle or tip due to the constant $V = dy_s/dt$ speed can be obtained as follows:

$$\begin{aligned}
&m^*_c \ddot{\zeta}_y + b_y \dot{\zeta}_y + k_y \zeta_y = F^c_y + F^c_z k_y/k_{yz} \ , \\
&m^*_c \ddot{\zeta}_z + b_z \dot{\zeta}_z + k_z \zeta_z = F^c_z + F^c_y k_z/k_{yz} \ , \\
&I_0 \ddot{\theta} = (f_{as} - f_{ta}) R_a \ , \\
&m_a \ddot{y} + b^*_{as} \dot{y} + k^*_{as} y = f_{as} + f_{ta} sin\beta - F_{ta} cos\beta \ , \\
&m_a \ddot{z} + b_{as} \dot{z} + k_{as} z = F_{as} - F_{ta} sin\beta - f_{ta} cos\beta \ , \\
&f_{as} = F_{ta} cos\beta - f_{ta} sin\beta \ , \\
&F_{as} = F_{ta} sin\beta + f_{ta} cos\beta \ , \\
&F^c_y = k_y cos\alpha y - F_{ta} cos\gamma + f_{ta} sin\gamma \ , \\
&F^c_z = k_z sin\alpha y - F_{ta} sin\gamma - f_{ta} cos\gamma \ , \qquad (17)
\end{aligned}$$

where $I_0 = 2m_a R^2_a/5$ is the moment of inertia of the particle, and $\gamma = \beta - \alpha$. From these equalities, assuming no rolling ($\ddot{\theta} = 0$) and $h \approx 0$, at the steady state:

$$\begin{aligned}
&\zeta_y = ycos\alpha - (F^c_y/k_y + F^c_z/k_{yz}) \ , \\
&\zeta_z = ysin\alpha - (F^c_z/k_z + F^c_y/k_{yz}) \ , \\
&f_{as} = f_{ta} \ , \\
&F_{ta} = \mu_k(\mu^k_{ta} cos\beta A_{ta} + A_{as})/ \\
&(cos\beta/(1+sin\beta) - \mu^k_{as}(\mu^k_{ta} cos\beta + sin\beta)) \ , \\
&f_{ta} = F_{ta} cos\beta/(1+sin\beta) \ , \\
&y = \zeta_y cos\alpha + \zeta_z sin\alpha + \Delta y \ , \\
&\Delta y = (\zeta_y sin\alpha - \zeta_z cos\alpha) sin\beta cos\beta \ , \\
&\Delta z = (\zeta_y sin\alpha - \zeta_z cos\alpha) sin^2\beta \ , \\
&\tilde{\beta} = arctan\{(R_a sin\beta + \delta z)/(R_a cos\beta - \Delta y)\} \ , \\
&F_z = k_y \zeta_y sin\alpha - k_z \zeta_z cos\alpha \ , \\
&z = \delta(\tilde{\beta}) \ . \qquad (18)
\end{aligned}$$

3 Force-Controlled Pushing

Using the real-time ζ_z feedback during pushing, following force-controlled pushing strategies can be proposed: z-position , xy-position, or xyz-position controlled pushing. The xy-position controlled pushing control scheme

is shown in Figure 6. The main design variable is the reference (x_r, y_r) position value. For a 2-D pushing-based positioning (x_r, y_r) is selected as $(x(0), y(0))$ where $x(0)$ and $y(0)$ are the after automatic contact detection particle (x, y) position since the stage and particle move, and the cantilever tip behaves as the stopper. Here, H_{xy} function transforms the deflection and position data to the particle position (x_a, y_a) feedback such that:

$$H_{xy} = \begin{cases} (x,y) = (x_s, y_s) \ , & \text{if } t \leq t^*; \\ (x,y) = (x^o, y^o) \ , & \text{otherwise.} \end{cases} \quad (19)$$

Here, (x_s, y_s) is the stage xy-position, t^* is the particle-substrate separation instant, and (x^o, y^o) is the tip-particle pushing settling xy-position. t^* can be detected experimentally in real-time by observing ζ_z such that if ζ_z has a peak at time t, then $t^* = t$. However, (x^o, y^o) cannot be measured directly, and needed to be estimated from the pushing model. For example, using the previous models, y^o can be observed in the Figure 7 where x^o can be observed in the same way. However, depending on the special parameters, the behaviour of the (x, y) could be also periodic motion, which can be observed in the model and experiments. In this case, the mean of the periodic function can be used as the (x, y) information.

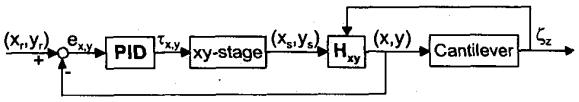

Figure 6: Force-controlled xy-positioning during particle pushing.

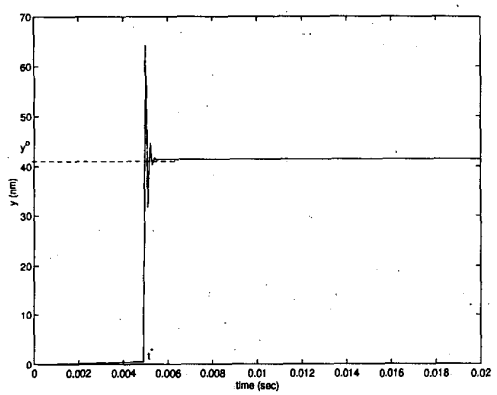

Figure 7: The settling of the y position of the particle during pushing.

4 System Setup

For conducting experiments, a home-made open-structure AFM system with Virtual Reality (VR) graphics display and haptic device is utilized [18]. Piezoresistive cantilevers where the cantilever has a doped silicon layer which changes its resistance due to the deflection moment are utilized. These type of cantilevers can be the future micro-robot grippers as the integrated sensor probes. Only the ζ_z is measurable with the present system. As the user interface, a graphics display as can be seen in Figure 8 which we call as VR Nano Visulator integrated with a 1-DOF haptic device is constructed. In the graphics display, scanned AFM images, and real-time cantilever tip position (spherical ball in the figure) are displayed. Using the haptic device, z-position of the tip can be controlled by the user with a real-time bilateral force feedback control. Thus, even there are positioning errors due to the piezoelectric stage on the visual display, the force-feedback enhances these types of errors.

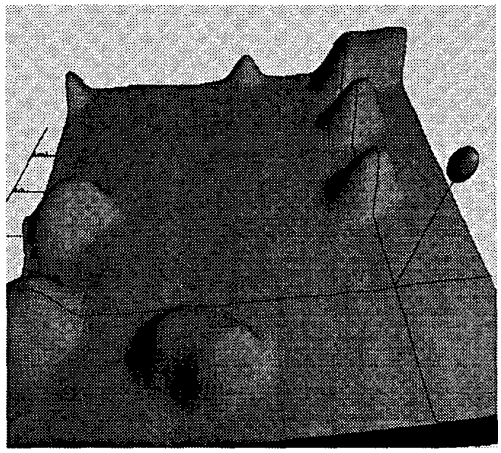

Figure 8: VR Nano Visulator display of 242 nm radius gold-coated latex nanoparticles during manipulation.

5 Experiments and Simulations

As the first experiment, the contact point detection is tested. The cantilever parameters are $R_t = 30\ nm$, and $k_c = 8\ N/m$, $L_x = 50\ \mu m$, $L_y = 155\ \mu m$, and $L_z = 6.5\ \mu m$. The motion speed is around $V = 2\ \mu m/sec$ with $\Delta = 0.1\ \mu m$ steps. During the particle-tip contact as can be seen in Figure 9, $-0.2\ V$ is the no deflection line where around the 43^{th} step of motion the particle contacts and bends until to $-1.5\ V$ which is the ζ_{set} for automatic contact detection. At this point stage stops moving.

Using the proposed models, the effect of different parameters cantilever deflection, and particle position is tried to be understood. During the simulations, if that parameter is not the changing one, the parameter values are selected as follows: $k_z = 8N/m$, $\mu^s_{as} = \mu^s_{ta} = 0.3$, $\mu^k_{as} = \mu^k_{ta} = 0.2$, $R_a = 1\ \mu m$, $R_t = 30\ nm$, $V = 1\ \mu m/sec$, $L_y = 155\ \mu m$, $L_z = 6.7\ \mu m$, $\alpha = 15^o$, $\beta = 30^o$, $\gamma_L = 72\ mJ/m^2$, $\nu_s = 0.27$, $\nu_t = 0.3$, $E_s = 169\ GPa$, and $E_t = 70\ GPa$. Assuming only pure-sliding case and contact point between the tip and particle is $y = 0$, at

first, the effect of the cantilever tilt angle α is observed. Here and after, all y and ζ_z values are the settled steady state values in the graphs. From Figure 10, it can be seen that within a limited range of α, ζ_z and y increase with the increased angle. Secondly, changing β tip-particle contact angle values, it can be deduced from the Figure 11 that optimum β can result in minimum y motion of the particle with a detectable range of ζ_z. Moreover, μas^s effect is tested as shown in Figure 12. From the figure, μ_{as}^s value around $0.6 - 0.7$ results in an unstable y and ζ_z behaviour. Finally, the cange in R_a results in the effect as shown in Figure 13.

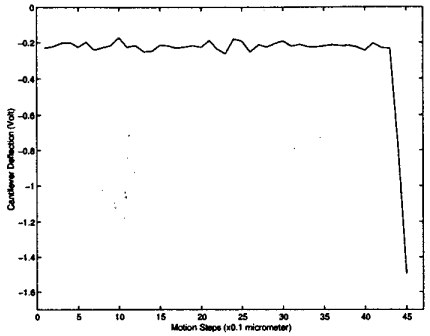

Figure 9: The experimental cantilever deflection during automatic contact detection.

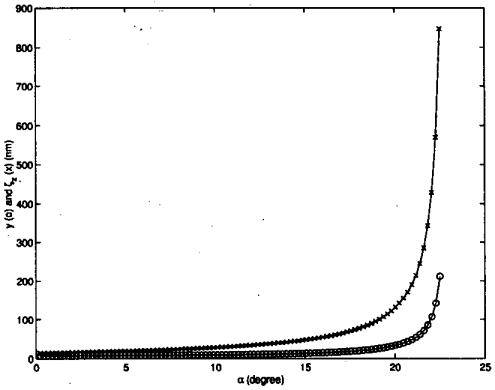

Figure 10: The effect of changing α on y ('o') and ζ_z ('x').

As the pushing experiment, 0.5 μm radius gold-coated latex particles are pushed in a task-based control user interface. The optical microscope images of an pushed particle example is given in Figure 14. During pushing, ζ_z measurement can be seen from the Figure 15. Since, the silicon surface is not perfectly flat, the deflection data is not horizontal, and it goes to zero by increasing the stage position. During pushing, there is a short stop interval around 32 μm position. It can be seen that the static friction peaks are clear from the data, and the periodic perturbations are due to the hardware and environment noise.

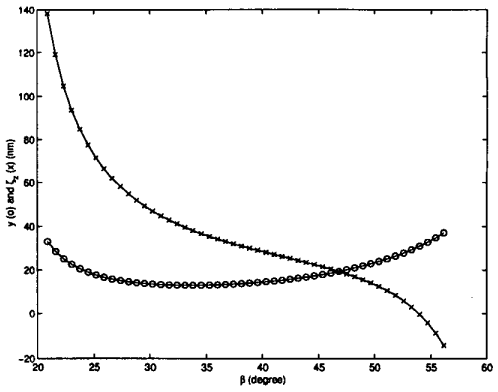

Figure 11: The effect of changing β on y and ζ_z.

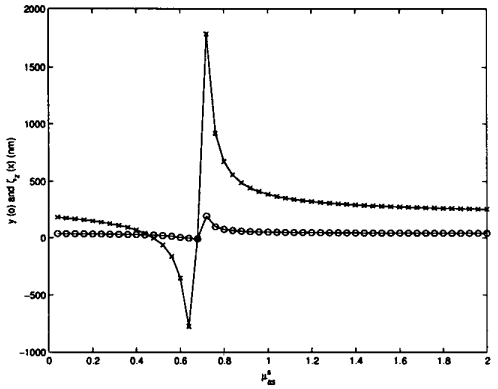

Figure 12: The effect of changing μ_{as}^s on y and ζ_z.

6 Conclusion

In this paper, a nanoparticle manipulation system using Atomic Force Microscope (AFM) as the manipulator has been proposed. Modeling and control of the AFM cantilever tip and particle interaction has been realized for moving particles with sizes less than 1 μm on a silicon substrate in 2-D. Particle manipulation experiments are realized, and it is shown that the system can be utilized in 2-D micro particle assembling. As the future work,

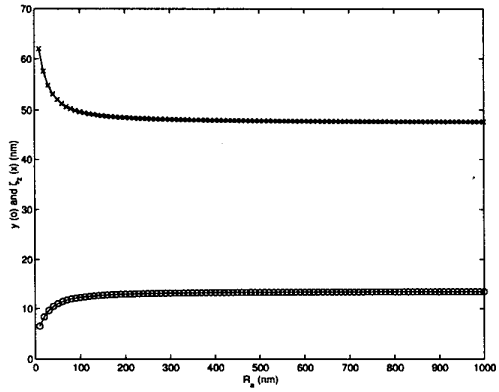

Figure 13: The effect of changing R_a on y and ζ_z.

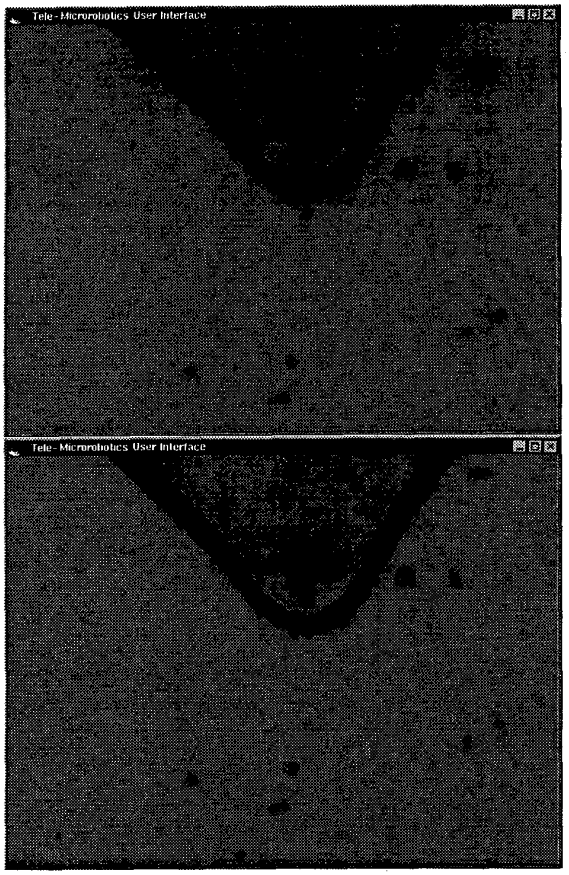

Figure 14: Pushing a 0.5 μm radius latex particle where the initial (upper image) and final positions (lower image) are shown using the high-resolution optical microscope top-view images.

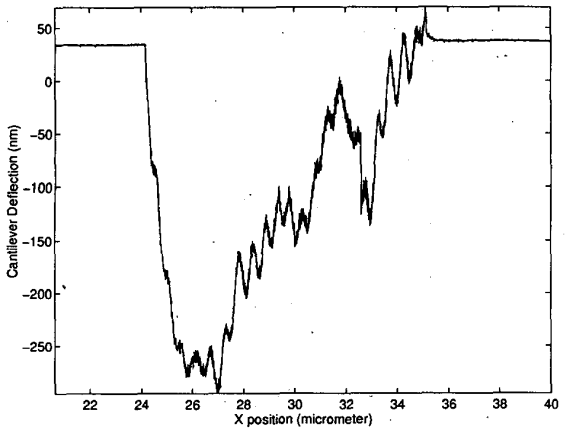

Figure 15: The cantilever deflection during pushing a particle around 12 μm distance with a brief stop at $x = 32\ \mu m$.

the manipulation operations will be realized in a liquid environment where the capillary and electrostatic forces are reduced.

References

[1] F. Arai, D. Ando, and T. Fukuda. Micro manipulation based on micro physics: Strategy based on attractive force reduction and stress measurement. In *Proc. of the IEEE Int. Conf. on Robotics and Automation*, pages 236–241, 1995.

[2] C. Baur, A. Bugaciv, and et al. Nanoparticle manipulation by mechanical pushing: Underlying phenomena and real-time monitoring. *Nanotechnology*, 9:360–364, 1998.

[3] J. Colchero, E. Meyer, and O. Marti. Friction on atomic scale. *Handbook of Micro/Nano Tribology, Second Ed., CRC Press*, pages 273–333, 1999.

[4] L. T. Hansen, A. Kuhle, and et al. A technique for positioning nanoparticles using an atomic force microscope. *Nanotechnology*, 9:337–343, 1998.

[5] T. R. Hicks and P. D. Atherton. *The Nano Positioning Book.* Queensgate Inst. Ltd., 1997.

[6] J. Israelachvili. *Intermolecular and Surface Forces.* Academic Press, 1992.

[7] T. Junno, K. Deppert, L. Montelius, and L. Samuelson. Controlled manipulation of nanoparticles with an atomic force microscopy. *App. Physics Letters*, 66(26):3627–3629, June 1995.

[8] T. Kasaya, H. Miyazaki, S. Saito, and T. Sato. Micro object handling under sem by vision-based automatic control. In *Proc. of the IEEE Int. Conf. on Robotics and Automation*, pages 2189–2196, 1999.

[9] T. Ondarcuhu and C. Joachim. Combing a nanofiber in a nanojunction. *Nanotechnology*, 1998 (to be appeared).

[10] U. Rabe, J. Turner, and W. Arnord. Analysis of the high-frequency response of atomic force microscope cantilevers. *Appl Phys. A*, 66:277–282, 1998.

[11] T. R. Ramachandran, C. Baur, and et al. Direct and controlled manipulation of nanometer-sized particles using the non-contact atomic force microscope. *Nanotechnology*, 9:237–245, 1998.

[12] A.A.G. Requicha, C. Baur, A. Bugacov, and et al. Nanorobotic assembly of two-dimensional structures. In *Proc. of the IEEE Int. Conf. on Robotics and Automation*, pages 3368–3374, 1998.

[13] R. Resch, C. Baur, and et al. Manipulation of nano particles using dynamic force microscopy: Simulation and experiments. *App. Phys. A*, 67(3):265–271, Sept. 1998.

[14] D. Sarid, J. P. Hunt, R. K. Workman, and et al. The role of adhesion in tapping-mode atomic force microscopy. *Appl. Phys. A*, (66):283–286, 1998.

[15] D.M. Schafer, R. Reifenberger, A. Patil, and R.P. Andres. Fabrication of two-dimensional arrays of nanometric-size clusters with the atomic force microscopy. *App. Physics Letters*, 66(8):1012–1014, Feb. 1995.

[16] M. Sitti and H. Hashimoto. Teleoperated nano scale object manipulation. In *Recent Advances on Mechatronics, ed. by O. Kaynak, S. Tosunoglu and M.J. Ang, Springer Verlag Pub., Singapore*, pages 322–335, 1999.

[17] M. Sitti and H. Hashimoto. Two-dimensional fine particle positioning using a piezoresistive cantilever as a micro/nano-manipulator. In *Proc. of the IEEE Int. Conf. on Robotics and Automation*, pages 2729–2735, Detroit, May 1999.

[18] M. Sitti and H. Hashimoto. Tele-nanorobotics using atomic force microscope. *Advanced Robotics Journal*, Fall 1999 (submitted).

[19] M. Sitti, Satoshi Horiguchi, and H. Hashimoto. Tele-touch feedback of surfaces at the micro/nano scale: Modeling and experiments. In *Proc. of the IEEE/RSJ Int. Conf. on Intelligent Robots and Systems*, Korea, Oct. 1999 (to be published).